

Wld^S Enhances Insulin Transcription and Secretion via a SIRT1-Dependent Pathway and Improves Glucose Homeostasis

Jingxia Wu,¹ Fang Zhang,¹ Menghong Yan,¹ Dongmei Wu,¹ Qiuqing Yu,¹ Yi Zhang,¹ Ben Zhou,¹ Michael W. McBurney,² and Qiwei Zhai¹

OBJECTIVE—Wld^S (Wallerian degeneration slow), a fusion protein from a spontaneous mutation containing full-length nicotinamide mononucleotide adenylyltransferase 1, has NAD biosynthesis activity and protects axon from degeneration robustly. NAD biosynthesis is also implicated in insulin secretion in β -cells. The aim of this study was to investigate the effect of Wld^S on β -cells and glucose homeostasis.

RESEARCH DESIGN AND METHODS—Using the Wld^S mice, we measured the expression of Wld^S in pancreas and analyzed the effect of Wld^S on glucose homeostasis. The direct effect of Wld^S on insulin transcription and secretion and the related mechanisms was measured in isolated islets or β -cell lines. Silent information regulator 1 (SIRT1), an NAD-dependent protein deacetylase, is involved in insulin secretion. Thus, Wld^S mice with SIRT1 deficiency were generated to study whether the SIRT1-dependent pathway is involved.

RESULTS—Wld^S is highly expressed in the pancreas and improves glucose homeostasis. Wld^S mice are resistant to high-fat diet-induced glucose intolerance and streptozotocin (STZ)-induced hyperglycemia. Wld^S increases insulin transcription dependent on its NAD biosynthesis activity and enhances insulin secretion. SIRT1 is required for the improved insulin transcription, secretion, and resistance to STZ-induced hyperglycemia caused by Wld^S. Moreover, Wld^S associates with SIRT1 and increases NAD levels in the pancreas, causing the enhanced SIRT1 activity to downregulate uncoupling protein 2 (UCP2) expression and upregulate ATP levels.

CONCLUSIONS—Our results demonstrate that Wld^S combines an insulinotropic effect with protection against β -cell failure and suggest that enhancing NAD biosynthesis in β -cells to increase SIRT1 activity could be a potential therapeutic approach for diabetes. *Diabetes* 60:3197–3207, 2011

From the ¹Key Laboratory of Nutrition and Metabolism, Institute for Nutritional Sciences, Shanghai Institutes for Biological Sciences, Chinese Academy of Sciences, Graduate School of the Chinese Academy of Sciences, Shanghai, China; and the ²Center for Cancer Therapeutics, Ottawa Hospital Research Institute, and Department of Medicine, University of Ottawa, Ottawa, Ontario, Canada.

Corresponding author: Qiwei Zhai, qwzhai@sibs.ac.cn.

Received 22 February 2011 and accepted 16 September 2011.

DOI: 10.2337/db11-0232

This article contains Supplementary Data online at <http://diabetes.diabetesjournals.org/lookup/suppl/doi:10.2337/db11-0232/-DC1>.

© 2011 by the American Diabetes Association. Readers may use this article as long as the work is properly cited, the use is educational and not for profit, and the work is not altered. See <http://creativecommons.org/licenses/by-nc-nd/3.0/> for details.

Glucose homeostasis is largely maintained by the pancreatic β -cells, which secrete insulin in response to elevated ATP levels as a result of glucose metabolism (1). β -Cell dysfunction often leads to diabetes (2,3). However, the underlying mechanisms involved in the preservation of β -cell function remain to be fully understood.

Silent information regulator 1 (SIRT1), an NAD-dependent protein deacetylase, regulates various biological processes including glucose homeostasis (4–6). SIRT1 controls the gluconeogenic/glycolytic pathways in the liver (7) and improves insulin sensitivity under insulin-resistant conditions in C2C12 myotubes (8). In β -cells, SIRT1 promotes the expression of NeuroD and MafA, two factors essential for the transcription of insulin, by deacetylating and activating Foxo1 to protect against oxidative stress (9). Moreover, glucose-stimulated insulin secretion (GSIS) in islets of SIRT1 knockout mice is blunted (10), whereas GSIS is enhanced in β -cell-specific SIRT1-overexpressing mice (11). Nevertheless, how SIRT1 is regulated to modulate insulin secretion and improve glucose homeostasis remains to be further explored.

Wallerian degeneration is an experimental model of axon degeneration. Remarkably, this degeneration is dramatically slowed in Wallerian degeneration slow (Wld^S) mice, a spontaneous mutant mouse strain (12). The protective function is attributed to a chimeric gene resulting from an 85 kb tandem triplication in chromosome 4 (13). The chimeric gene, Wld^S, encodes an N-terminal 70 amino acids fragment of ubiquitination factor E4B (Ube4b) fused to nicotinamide mononucleotide adenylyltransferase 1 (NMNAT1), a crucial enzyme for NAD biosynthesis (14,15). The NAD biosynthesis activity is pivotal for the neuronal protective function of Wld^S, which maintains the cellular NAD levels in a steady state and prevents NAD decline in injured axons (16,17). It has been implicated that NAD biosynthesis is also involved in β -cell function. The activity of SIRT1 on GSIS in β -cell-specific SIRT1-overexpressing mice decreases with age, which probably is the result of a decline in systemic NAD biosynthesis (18). Haplodeficiency of nicotinamide phosphoribosyltransferase (NAMPT) in female mice, but not male, causes the decrease of NAD biosynthesis and defect of GSIS, and the extracellular form of NAMPT seems to be the main causation (19). Thus, whether the enhancement of NAD biosynthesis mediated by Wld^S increases GSIS and improves glucose homeostasis remains to be elucidated.

In this study, we found that Wld^S mice showed improved glucose homeostasis even under high-fat (HF) diet and

streptozotocin (STZ)-challenged states and that Wld^S regulated insulin transcription and secretion dependent on SIRT1. Moreover, Wld^S associated with SIRT1 and increased NAD levels in the pancreas, which led to the enhanced SIRT1 activity to downregulate uncoupling protein 2 (UCP2) and upregulate ATP levels. Thus enhancing NAD biosynthesis in β -cells to increase SIRT1 activity might be a potential therapeutic approach for diabetes.

RESEARCH DESIGN AND METHODS

Animals. All mice were maintained and used in accordance with the guidelines of the Institutional Animal Care and Use Committees at the Institute for Nutritional Sciences. Wld^S mice (C57BL/6 background) were purchased from Harlan. C57BL/6 mice and imprinting control region (ICR) mice were purchased from Slac (Shanghai, China). SIRT1^{+/-} mice (129/Sv background) were described previously (20). SIRT1^{+/-} mice were crossed with ICR mice to get SIRT1^{+/-} mice on an outbred genetic background. We then mated Wld^S mice with SIRT1^{+/-} mice (129/ICR background) and intercrossed the double-heterozygous SIRT1^{+/-} Wld^{S/+} mice to obtain SIRT1^{+/+} Wld^{S-/-}, SIRT1^{+/-} Wld^{S/+}, SIRT1^{-/-} Wld^{S/+}, and SIRT1^{-/-} Wld^{S-/-} mice. The genotyping for Wld^S and SIRT1 was carried out as described previously (20,21).

Islet morphology analysis. The islet area and the islet cell density were determined as described previously (22). All measurements were made using a fluorescence microscope (BX61; Olympus) and Image-Pro Plus software (version 5.0.1; Media Cybernetics). At least four mice and 40 islets per mouse were studied for each group.

Immunofluorescence. Pancreatic fresh-frozen sections of 16-week-old mice or fixed cells were incubated overnight at 4°C with indicated antibodies including anti-mouse insulin antibody (Sigma), anti-Wld^S antibody (a gift from Dr. Michael P. Coleman, The Babraham Institute), and rabbit anti-Myc antibody (Santa Cruz Biotechnology) and then detected with Alexa Fluor 555 goat anti-rabbit IgG and/or Alexa Fluor 488 goat anti-mouse IgG antibodies (Molecular Probes). DAPI (Sigma) was used to stain the nuclei. Immunofluorescence images were obtained on a Zeiss LSM 510 META confocal microscope or an Olympus IX51 fluorescence microscope.

Glucose, insulin, C-peptide, homeostasis model of insulin resistance, and homeostasis model of β -cell measurements. Fed glucose and insulin levels were measured about 3 h after light on. Fasted glucose, insulin, and C-peptide levels were measured after 17-h fasting. The refed blood glucose levels were measured in the mice refed for 2 h after a 17-h fasting. Tail blood was collected to measure glucose with a glucometer (FreeStyle), to measure insulin levels by a radioimmunoassay kit (Beijing North Institute of Biological Technology, China), or to measure C-peptide by an ELISA kit (Millipore). Homeostasis model of insulin resistance (HOMA-IR) and homeostasis model of β -cell function values were obtained using the HOMA Calculator v2.2 (23).

Glucose tolerance and insulin tolerance tests. Glucose tolerance tests were performed on male mice fasted 13 h. Glucose concentrations were measured in blood collected by venous bleeding from the tail vein at the indicated times after an intraperitoneal injection of glucose (2 g/kg body wt). Insulin tolerance tests were performed on male mice fasted for 4 h (9:00–13:00). Glucose levels were likewise measured from tail blood after an intraperitoneal injection at 0.75 units/kg body weight of human insulin (Eli Lilly).

HF diet-induced obesity mouse model. Five-week-old Wld^S and wild-type mice were randomly assigned and fed with either normal chow containing 10 kcal% fat or HF diet containing 45 kcal% fat (Research Diets). After mice were fed for 12 weeks, fat and lean mass were measured in conscious animals by a minispec mq serial NMR spectrometer (Bruker). Serum total cholesterol, HDL-cholesterol, and LDL-cholesterol levels were determined by enzymatic assays on an Olympus automated analyzer.

Multiple low-dose STZ (MLDS) treatment in vivo. Ten-week-old male mice were injected intraperitoneally for 5 consecutive days with 40 mg/kg STZ (Sigma) freshly prepared in cold 0.1 mol/L citrate buffer (pH 4.5) as described previously (24). Blood glucose was monitored weekly, and the mice were considered diabetic when their blood glucose levels were over 250 mg/dL in 2 consecutive weeks. Pancreata were frozen in liquid nitrogen and processed for frozen sections and immunohistochemistry. The percentage of insulin area was quantified as described previously (25).

Immunohistochemistry. After being fixed with ice-cold acetone, frozen sections were treated with 3% H₂O₂ to block the endogenous peroxidase. Anti-mouse insulin antibody was from Sigma. Biotinylated goat anti-mouse IgG (Jackson ImmunoResearch) and Streptavidin-HRP (Zymed) were used to amplify the signal, and diaminobenzidine (DAB) was used as chromogen.

Plasmids. pCMV-Wld^S and pCMV-Wld^S-F116S were constructed as described previously (26). pCMV-NMNAT1 and pCMV-NMNAT1-F28S were constructed by insertion of NMNAT1 or NMNAT1-F28S cDNA fragment amplified from

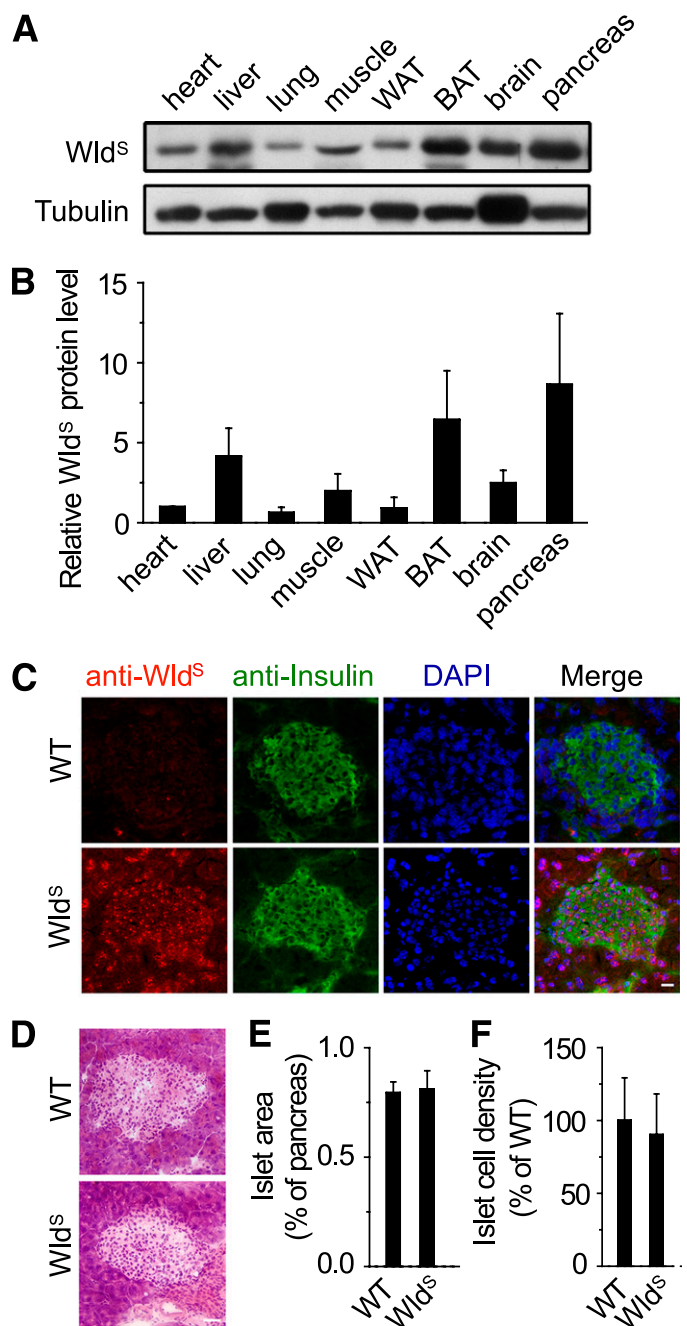


FIG. 1. Wld^S protein is highly expressed in pancreatic β -cells and has no effect on the morphology of islets. **A:** Wld^S protein levels of the indicated tissues were determined by Western blot. Tubulin was used as a loading control. WAT, white adipose tissue; BAT, brown adipose tissue. **B:** Quantification of Wld^S protein levels in **A**. Except where indicated, in this and all other figures, error bars represent SD. **C:** The expression of Wld^S in frozen pancreatic sections of the indicated genotypes was measured by immunofluorescence using antibodies against Wld^S and insulin. DAPI was used to visualize the nuclei. Scale bar, 20 μ m. **D:** Hematoxylin and eosin staining of the pancreatic sections. Scale bar, 40 μ m. **E and F:** Percentage of islet area (**E**) and islet cell density (**F**) in 16-week-old Wld^S mice were similar to wild-type (WT) mice ($n = 4$ for each genotype). (A high-quality digital representation of this figure is available in the online issue.)

pCMV-Wld^S or pCMV-Wld^S-F116S into pCMV-tag3A vector (Stratagene), respectively, using the primers including GCTGAAGCTTGATCACAGAGTGGAA-TGGTTG and CAGCGGATCCTATGGACTCATCCAAGAAG. pEGFP (enhanced green fluorescent protein)-Wld^S was constructed by insertion of Wld^S cDNA fragment amplified from pCMV-Wld^S into pEGFP-C3 vector (Clontech) using the primers including CTGCAAGCTTATGGAGGAGCTGAGCGCTGAC and

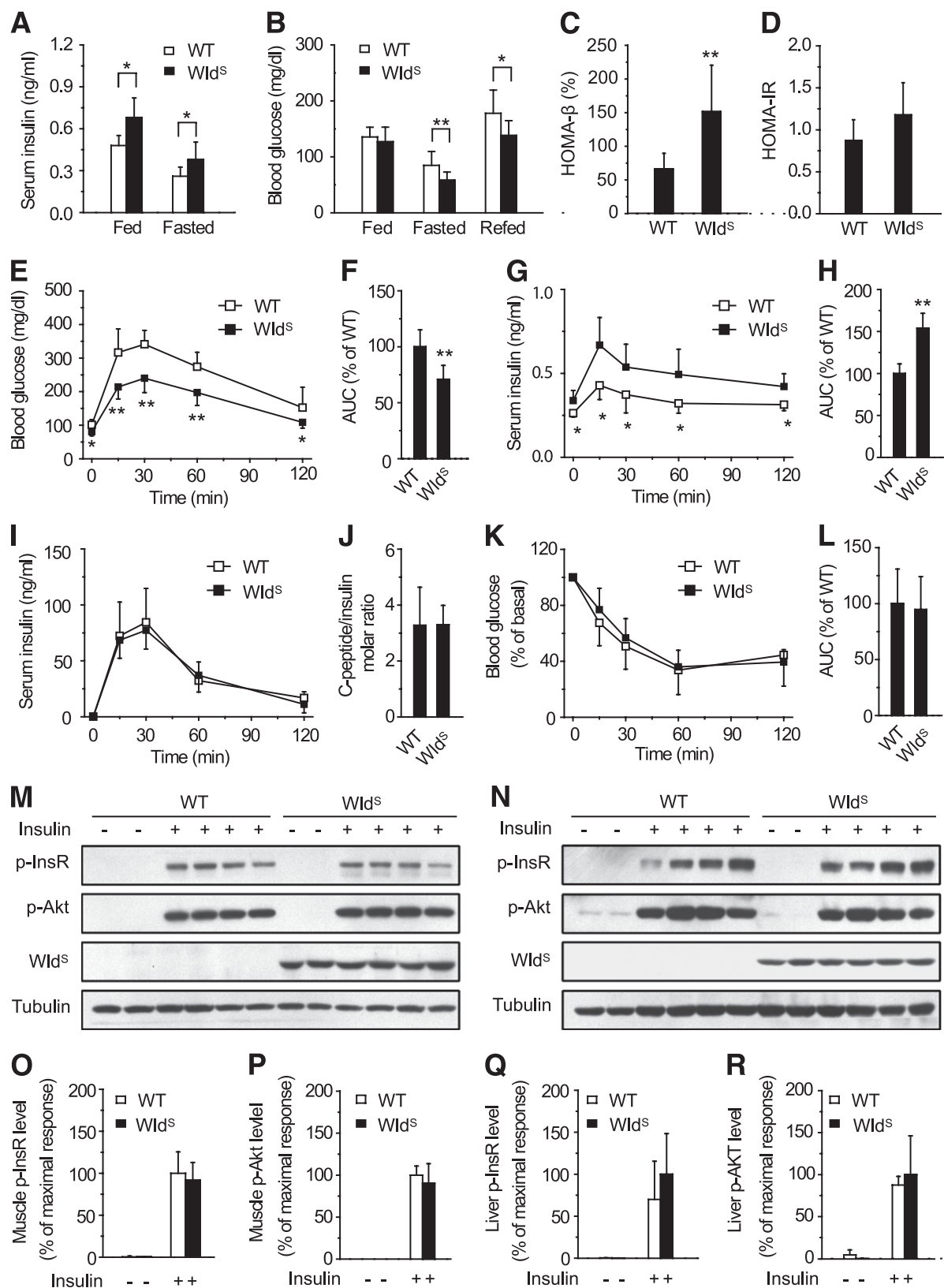


FIG. 2. Wld^S mice show increased serum insulin levels, improved glucose tolerance, normal insulin clearance rate, and normal insulin sensitivity. **A:** Serum insulin levels of Wld^S mice ($n = 9$) were significantly higher than those of wild-type (WT) ($n = 10$) no matter whether they were fed ad libitum or fasted overnight. Except where indicated, in this and all other figures, $*P < 0.05$ and $**P < 0.01$. **B:** Blood glucose levels of 13-week-old Wld^S mice ($n = 16$) were significantly lower than those of wild-type ($n = 24$) when fasted overnight or refed for 2 h after fasting. **C:** HOMA-β (homeostasis model of β-cell function) index of Wld^S mice ($n = 9$) was higher than that of wild-type ($n = 10$). **D:** HOMA-IR (homeostasis model of insulin resistance) index of Wld^S mice ($n = 9$) was similar to that of wild-type ($n = 10$). **E:** Wld^S mice showed improved glucose tolerance compared with wild-type as determined by glucose tolerance test (22-week-old; $n = 14$ to 15 for each group). **F:** Area under the curve (AUC) of the glucose tolerance test in (**E**). **G:** Serum insulin levels in Wld^S mice were higher than those in wild-type mice during the glucose tolerance test (22-week-old);

GTCTGGGATCCCGTCACAGAGTGAATGGTTG. pEGFP-Wld^S-H112A was engineered by using Quick Change II Site-Directed Mutagenesis Kit as described by the instruction manual (Stratagene) using the primers CCCATCACCAACATGGCCCTCAGGCTGTTCAG and CTCGAACAGCCTGAGGGCCATGTTG-GTGATGGGG. pGL3-Insulin-Promoter was constructed by insertion of 340 bp fragment of rat insulin I 5' flanking region into the *SacI* and *BglII* sites of pGL3-basic vector (Promega) using the primers CCGAGCTCCCCTCCAAATGTTCTTCTTCTGG and GCGAGATCTGGGAGTTACTGGGTCTCCACTA. pGL3-UCP2-Promoter was constructed by insertion of 800 bp fragment of mouse UCP2 promoter into *XhoI* and *KpnI* sites of pGL3-basic vector using the primers CATATGGTACCAGCCTAATTCCTAGGCAAGC and GATTCTCGAG-GCGGAACTGACAGTAGCTGCGAAC. pCMV-myc-SIRT1 was constructed by insertion of SIRT1 cDNA fragment cut from pCS2+-Sirt1 (27) into pCMV-tag3A at the *BamHI* site. pCMV-PPAR γ 2 was constructed by insertion of PPAR γ 2 cDNA amplified from pSG5-PPAR γ 2 (a gift from Dr. Ronald M. Evans, the Salk Institute) into pCMV-tag3A at the *SalI* and *XhoI* sites using the primers CCTCGTCGACTATGGGTGAAACTCTGGGA and CGCCTCGAGCCCTAGTAC-AAGTCTTGTAGATC.

Establishment of stably transfected cell lines. MIN-6 cells were transfected with pEGFP-C3, pEGFP-Wld^S, pEGFP-Wld^S-H112A, pCMV-tag3A, pCMV-Wld^S, and pCMV-Wld^S-F116S, respectively, using Lipofectamine 2000 (Invitrogen). Twenty-four hours after transfection, the cells were treated with 280 μ g/mL G418 (Sigma). Days (4–7) later, the living cells were diluted to 96-well plates to obtain monoclonal cells. The monoclonal MIN6 cells with stable expression of the indicated proteins were then amplified and confirmed by Western blot and immunofluorescence.

Measurement of NMNAT enzyme activity and luciferase assay. The NMNAT enzyme activity was measured as described previously (26). To measure insulin promoter activity, INS-1 cells (a generous gift from Dr. Christopher B. Newgard, Duke University Medical Center) in 24-well plates were cotransfected with 0.1 μ g pGL3-Insulin Promoter, 0.1 μ g pSV40- β -gal, and 0.8 μ g indicated plasmids per well using Lipofectamine 2000 (Invitrogen). To evaluate UCP2 promoter activity, 293T cells in 24-well plates were transiently cotransfected with 0.1 μ g pGL3-UCP2-Promoter, 0.1 μ g pSV40- β -gal, and 0.8 μ g indicated plasmids. The transfected plasmids were balanced with empty vector, and the total amount of transfected plasmids was 1 μ g per well. After transfection for 40 h, cells were harvested and measured with a luciferase assay kit (Promega) and normalized to β -galactosidase activity as described previously (28).

Islet isolation, glucose-stimulated insulin secretion, insulin, and ATP content. Islets were isolated by collagenase P (Roche) digestion as described previously (11). Ten handpicked islets per well with similar average size were cultured in 24-well plates overnight in RPMI 1640 containing 11 mmol/L glucose, 2 mmol/L L-glutamine, and 10% FBS. The islets were then preincubated in Krebs-Ringer bicarbonate buffer for 1 h at 37°C and subsequently stimulated with 2 mmol/L glucose, 20 mmol/L glucose, or 20 mmol/L KCl plus 2 mmol/L glucose in Krebs-Ringer bicarbonate buffer in triplicate for 2 h. The supernatant was collected for insulin measurements.

The remaining islets were washed twice with PBS and then extracted with ethanol-water-concentrated HCl (750:235:15) overnight at 4°C to measure insulin content by radioimmunoassay or mixed with 9 volumes of boiling Tris/EDTA buffer (0.1 mol/L Tris-acetate and 2 mmol/L EDTA [pH 7.75]) and raised to the boiling point again for 60–90 s to measure ATP levels. After cooling, ATP levels were measured using an ATP Bioluminescent Assay Kit (Promega) and normalized to the protein content.

Real-time quantitative PCR. Total RNA was prepared from isolated primary islets and stably transfected MIN6 cells by TRIzol reagent (Invitrogen) and reverse transcribed to cDNA. Real-time quantitative PCR was performed with ABI Prism 7900 sequence detection system using Power SYBR Green PCR Master Mix (Applied Biosystems) with primers TGGAGGCTCTCTACCTGGTG and TCTACAATGCCACGCTTCTG for insulin, GGTCCGCTTCCAGGCTCAGG and ATTACGGCAACATTGGGAG for UCP2, CACGACTTGCTGGTGGACAG and GTCTTGGCCAGCTCGAAC for Wld^S, GCTGACGACTCGACGACG and TCGGTCAACAGGAGGTTGTCT for SIRT1, CATGGATGACGATATCGCTGC and GTACGACCAGAGGCATACAGG for β -actin, TCCTTCCTCGTGCCGTACAT

and GTGGTCTCACCAGCTCTGA for Ube4b, and CCTCAAGGCCTGACAA-CAT and CCACAGGCCAGGAGAACCAC for NMNAT1. Quantification of mRNA copy numbers was performed as described previously (29).

Coimmunoprecipitation and Western blot. Coimmunoprecipitation was carried out as described previously (28). The supernatant of cell or pancreas lysates was collected for coimmunoprecipitation with the indicated primary antibody. For Western blot, 20-week-old mice of the indicated genotypes were killed and the indicated tissues were removed and snap-frozen. Tissue homogenates were made with radioimmunoprecipitation assay buffer and used for Western blot analysis. Protein samples were analyzed with antibodies against SIRT1 (Upstate), InsR, Tyr1150/1151-phosphorylated InsR, Ser473-phosphorylated Akt, Ser9-phosphorylated GSK-3 β (Cell Signaling), UCP2 (Calbiochem), α -tubulin, β -actin, NMNAT1 (Sigma), and Wld^S. Each blot shown in the figures is representative of at least three experiments. Quantification was performed by Image-Pro Plus software (version 5.0.1; Media Cybernetics).

NAD, nicotinamide adenine mononucleotide (NMN), nicotinamide (NAM), nicotinic acid (NA), NADP, NADH, and NADPH measurement. All compounds were extracted and analyzed as described previously (30,31). In brief, about 30 mg of frozen pancreas tissue was homogenized in acid extraction buffer to extract NAD, NMN, NA, and NADP or in alkali buffer to extract NAM, NADH, and NADPH. The samples were then analyzed using a liquid chromatography-tandem mass spectrometry with an Agilent 1200 series high-performance liquid chromatography system and a 4000 Q Trap tandem mass spectrometer (Applied Biosystems). The data analysis was done with the Applied Biosystems Analyst software 1.4.2.

Metabolic rate and physical activity. Oxygen consumption, carbon dioxide output, respiratory exchange ratio, and locomotor activity were determined for male mice fed ad libitum at 13 to 14 weeks of age using Comprehensive Laboratory Animal Monitoring System (CLAMS; Columbus Instruments) according to the manufacturer's instructions. Animals were acclimated to the system for 16–20 h and then measured during the next 24 h. Locomotor activity was derived from the sum of *x* and *z* axis beam breaks monitored every 15 min.

Statistics. Except where indicated, data are expressed as mean \pm SD of at least three independent experiments, and statistical significance was assessed by Student's *t* test. Differences were considered statistically significant at *P* < 0.05.

RESULTS

Wld^S protein is highly expressed in pancreas and has no effect on the morphology of islets. We found Wld^S was expressed in various tissues, and highly expressed in pancreas including insulin-producing β -cells (Fig. 1A–C and Supplementary Fig. 1A). The presence of Wld^S did not change the mRNA levels of Ube4b or NMNAT1 (Supplementary Fig. 1B and C) or the NMNAT1 protein levels (Supplementary Fig. 1D–H). The Wld^S mRNA level exceeded that of NMNAT1 by more than 20-fold in the pancreas (Supplementary Fig. 1I). The islet area and islet cell density were unaltered by Wld^S (Fig. 1D–F). These data show that the high expression of Wld^S has no significant effect on the morphology of islets.

Wld^S mice show high levels of serum insulin, improved glucose tolerance, normal insulin clearance rate, and normal insulin sensitivity. Next we investigated whether Wld^S had any effect on β -cell function. Serum insulin levels in 13-week-old Wld^S mice were higher than those of wild-type in both fed and fasted animals (Fig. 2A). Fed blood glucose levels were similar in wild-type and Wld^S mice, but fasted and refed blood glucose levels in Wld^S mice were significantly lower (Fig. 2B). Similar effects of Wld^S on fed

n = 8 for each group). *H*: AUC of the serum insulin levels in *G*. *I*: Serum insulin levels after intraperitoneal injection of 10 units/kg human insulin in chow-fed wild-type and Wld^S mice at the indicated time points (17-week-old; *n* = 8 for each group). *J*: The fasting C-peptide-to-insulin molar ratio was similar between wild-type and Wld^S mice (18-week-old; *n* = 7 for each group). *K*: Insulin tolerance in 23-week-old wild-type and Wld^S mice was similar as determined by insulin tolerance test (*n* = 8 for each group). *L*: AUC of the insulin tolerance test in *K*. *M* and *N*: Insulin sensitivity was similar in 24-week-old Wld^S and wild-type mice as determined by *in vivo* phosphorylation assay with the muscle (*M*) or liver (*N*) samples using phospho-Tyr1150/1151-InsR (*p*-InsR), phospho-Ser473-Akt (*p*-Akt), Wld^S, and tubulin antibodies. Male Wld^S (24-week-old) and wild-type mice were fasted for 16 h, anesthetized, and injected with PBS or human insulin (5 units/kg) through their inferior vena cava. The liver and muscle samples were collected 5 and 10 min after injection of insulin, respectively, and snap-frozen in liquid nitrogen for subsequent Western blot analysis. *O*–*R*: Quantification of the muscle and liver phospho-Tyr1150/1151-InsR and phospho-Ser473-Akt protein levels corresponding to *M* and *N*.

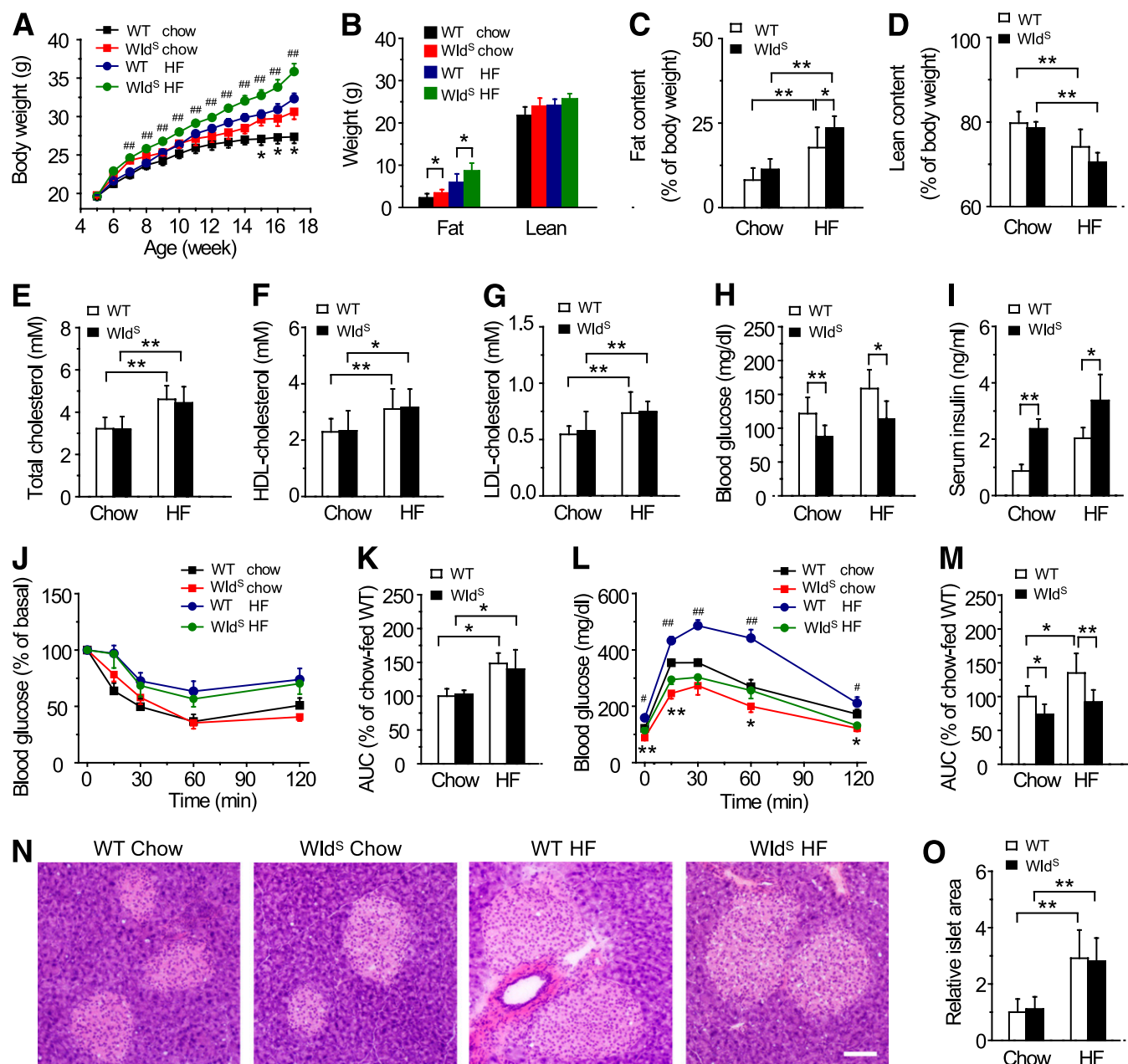


FIG. 3. Wld^S mice show improved glucose tolerance when fed HF diet. **A:** Weekly body weight of wild-type (WT) and Wld^S mice fed chow or HF diet from 5 to 17 weeks old. Except where indicated, $n = 6-8$ for each group in all panels of Fig. 3. Error bars indicate SEM. * $P < 0.05$ vs. Wld^S mice fed chow; ## $P < 0.01$ vs. wild-type fed HF diet. **B:** Fat and lean mass of 16-week-old wild-type and Wld^S mice fed chow or HF diet. **C** and **D:** Fat content was increased and lean content was decreased in both wild-type and Wld^S mice after feeding with 12-week HF diet. **E-G:** Serum total cholesterol, HDL-cholesterol, and LDL-cholesterol levels were elevated in both groups after feeding with 12-week HF diet, and no significant difference was observed between wild-type and Wld^S mice. **H** and **I:** Wld^S mice showed significantly decreased fasting blood glucose (**H**) and increased serum insulin levels (**I**) compared with wild-type no matter whether mice were fed chow or HF diet (24-week-old, HF diet fed for 19 weeks). **J:** Mice fed HF diet (22-week-old) showed decreased insulin tolerance compared with those fed chow, but no significant difference was observed between wild-type and Wld^S mice no matter whether mice were fed chow or HF diet. Error bars indicate SEM. **K:** AUC of the insulin tolerance test in **J**. **L:** Wld^S mice showed improved glucose tolerance compared with wild-type no matter whether mice were fed chow or HF diet (21-week-old, HF diet fed for 16 weeks). Error bars indicate SEM. * $P < 0.05$, ** $P < 0.01$, vs. wild-type fed chow; # $P < 0.05$, ## $P < 0.01$ vs. Wld^S mice fed HF diet. **M:** AUC of the glucose tolerance test in **L**. **N:** Hematoxylin and eosin staining of the pancreatic sections of wild-type and Wld^S mice fed chow or HF diet for 19 weeks. Scale bar, 100 μm . **O:** The islet area of Wld^S and wild-type mice fed HF diet was enlarged to a similar extent ($n = 4$ for each genotype). (A high-quality color representation of this figure is available in the online issue.)

serum insulin and fasted blood glucose levels were also observed in mice with a mixed genetic background (C57/129/ICR), and the effects in heterozygous Wld^S mice were weaker than the homozygous ones (Supplementary Fig. 2A and B). Furthermore, homeostasis model of β -cell function of 13-week-old Wld^S mice was significantly upregulated (Fig. 2C), and HOMA-IR was similar (Fig. 2D). Wld^S mice

showed markedly improved glucose tolerance (Fig. 2E and F), and these effects were dependent on the gene dose of Wld^S and decreased with age (Supplementary Fig. 2C-E). Serum insulin levels of Wld^S mice during the glucose tolerance test were significantly higher than those of wild-type (Fig. 2G and H), suggesting the improved β -cell function in Wld^S mice. Insulin clearance rate was not

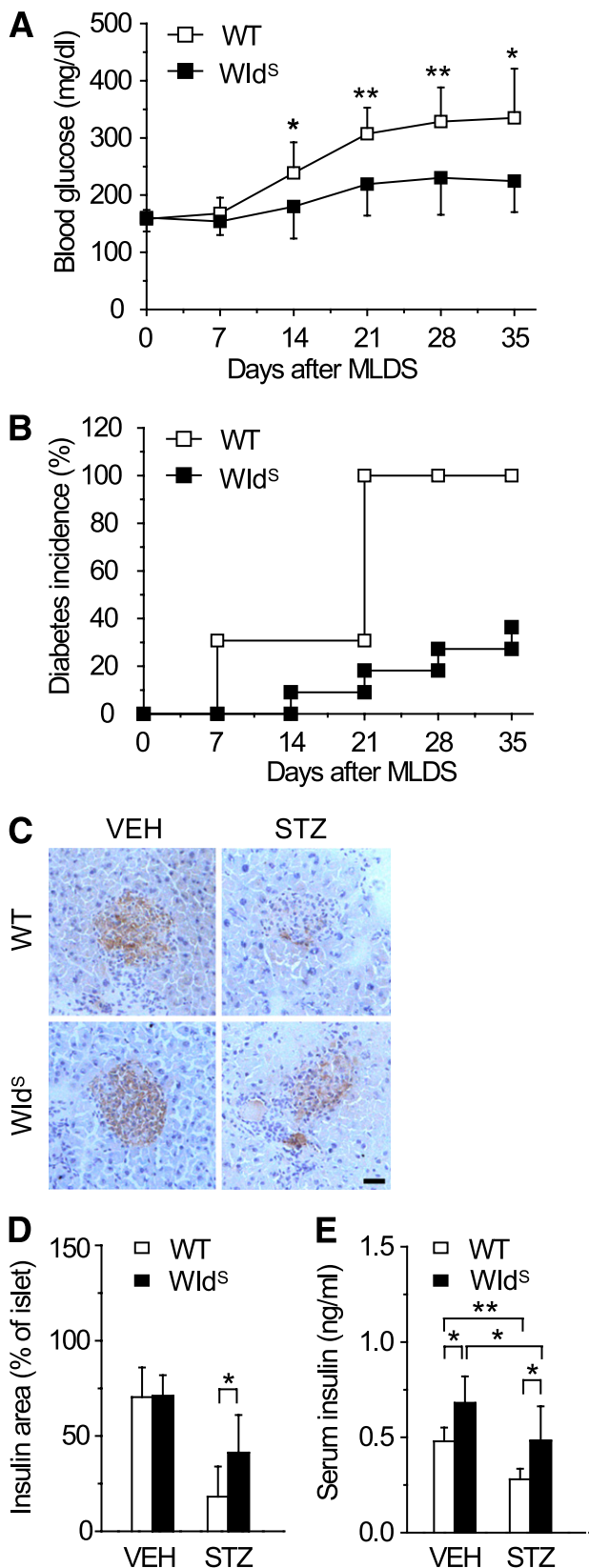


FIG. 4. Wld^S mice are resistant to STZ-induced hyperglycemia. **A** and **B**: Blood glucose levels and diabetes incidence of Wld^S mice ($n = 11$) were lower than those of wild-type (WT) mice ($n = 14$) after MLDS treatment at the indicated times. For diabetes incidence, $P < 0.001$ by Log-rank test. **C**: Immunostaining of pancreatic sections from wild-type and Wld^S mice using anti-insulin antibody 35 days after vehicle (VEH) or MLDS treatment. Hematoxylin staining was performed after immunostaining. **D**: The percentage of insulin positive area in islets of Wld^S mice was

affected by Wld^S when monitored by in vivo insulin clearance assay and fasting C-peptide-to-insulin molar ratio (Fig. 2I and J), which indicated that the elevated serum insulin levels in Wld^S mice were not a result of altered insulin clearance. Insulin tolerance test confirmed that Wld^S and wild-type mice had similar insulin sensitivity as measured by HOMA-IR (Fig. 2K and L). Insulin-induced phosphorylation of insulin receptor and AKT in muscle and liver was also indistinguishable between Wld^S and wild-type mice (Fig. 2M-R). In addition, the protein level of SIRT1, an important regulator in hepatic metabolism, and NAD levels in the liver were similar in wild-type and Wld^S mice (Supplementary Fig. 3A-C). These data show that Wld^S improves β -cell function and glucose homeostasis but does not affect insulin sensitivity.

Wld^S mice show improved glucose tolerance when fed HF diet. The body weight and fat mass were moderately increased in Wld^S mice compared with wild-type when fed chow, and the differences were more prominent when fed HF diet (Fig. 3A and B). As expected, HF diet caused increased fat content and decreased lean content in both groups (Fig. 3C and D). Interestingly, when compared with wild-type mice, the fat content was increased in Wld^S mice fed HF diet (Fig. 3C). Serum total cholesterol, HDL-cholesterol, and LDL-cholesterol levels were elevated in both groups fed HF diet for 12 weeks, and no differences were observed between wild-type and Wld^S mice (Fig. 3E-G). In Wld^S mice fed with either chow or HF diet, fasting blood glucose levels were decreased, and serum insulin levels but not insulin sensitivity was remarkably increased, compared with corresponding wild-type controls (Fig. 3H-K). Notably, wild-type mice fed HF diet exhibited impaired glucose tolerance, and this was strikingly improved in Wld^S mice (Fig. 3L and M). The islet area of Wld^S and wild-type mice fed HF diet was enlarged to a similar extent (Fig. 3N and O). These data suggest that Wld^S alleviates HF diet-induced glucose intolerance by enhancing insulin production.

Wld^S ameliorates STZ-induced hyperglycemia in mice. To study the direct effect of Wld^S on β -cells, mice were administered STZ, which selectively destroys β -cells (32). After MLDS treatment, blood glucose levels in both groups increased gradually, but were much lower in Wld^S mice than those in wild-type (Fig. 4A). The diabetes incidence in Wld^S mice was only about 18% compared with 100% in wild-type 21 days after MLDS treatment, and these trends were maintained thereafter for at least 14 days (Fig. 4B). After MLDS treatment, Wld^S mice preserved more insulin producing β -cells and remarkably higher serum insulin levels than wild-type (Fig. 4C-E). These data show that Wld^S protects against pancreatic β -cell failure and hyperglycemia induced by MLDS.

Wld^S enhances insulin transcription and secretion. We next investigated how Wld^S enhanced insulin production. As shown in Fig. 5A and B, islets isolated from Wld^S mice released more insulin under basal, glucose-, or KCl-stimulated conditions than those from wild-type when normalized to either the protein concentration or the insulin content. Wld^S mainly localized in the nuclear of islet β -cells, when treated with glucose or KCl (Supplementary Fig. 4).

higher than that of wild-type corresponding to C. E: Serum insulin levels of Wld^S mice were higher than those of wild-type 35 days after vehicle or MLDS treatment. $n = 8-13$ for each group. * $P < 0.05$ and ** $P < 0.01$. (A high-quality digital representation of this figure is available in the online issue.)

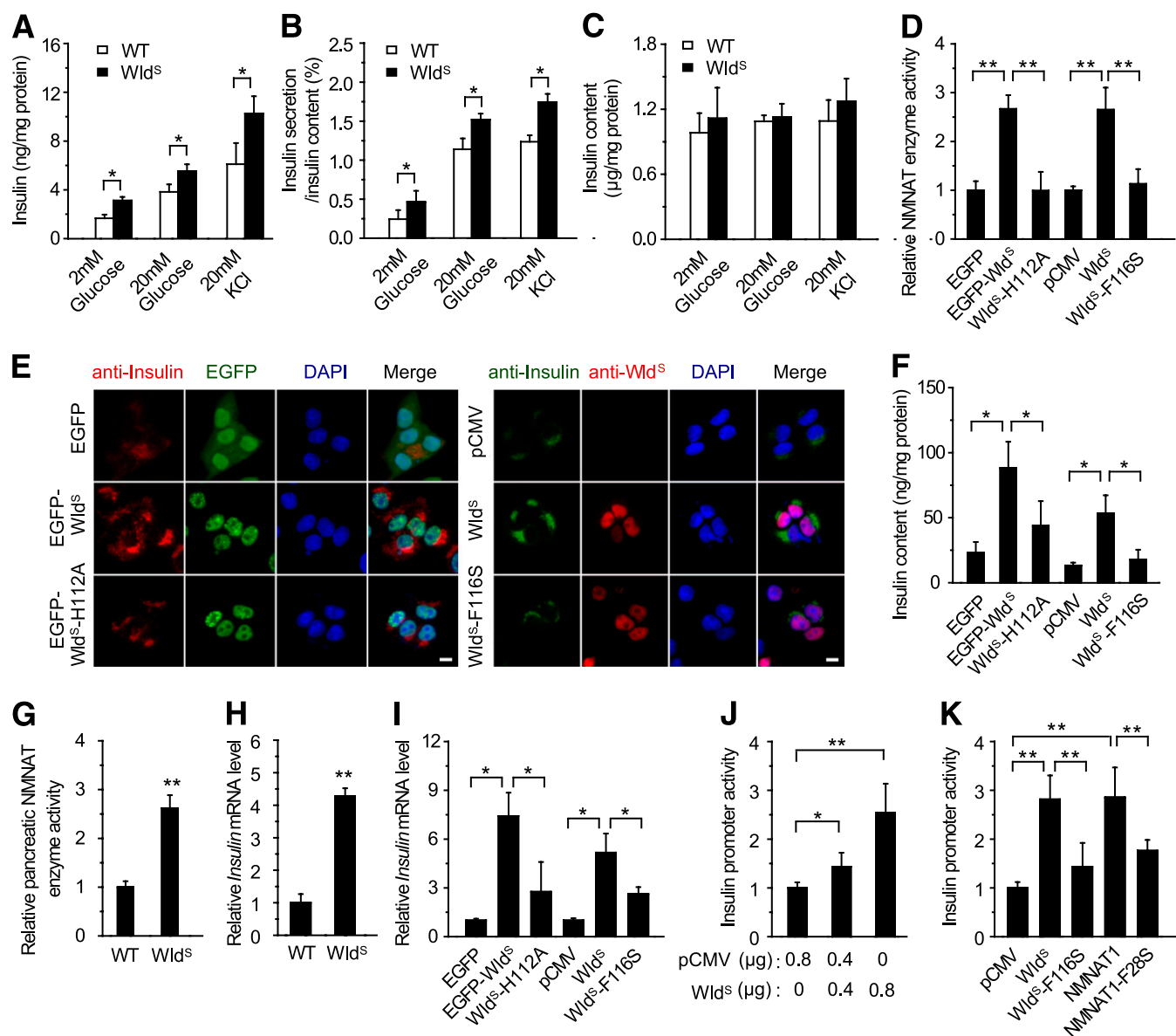


FIG. 5. Wld^S enhances insulin transcription and secretion. **A** and **B**: Insulin secretion of islets isolated from Wld^S mice was upregulated compared with wild-type (WT) when treated with the indicated concentration of glucose or KCl ($n = 7$ for glucose stimulation and $n = 4$ for KCl stimulation). The protein concentration (**A**) and the insulin content (**B**) were measured as internal control, respectively. **C**: Insulin content in the islets of Wld^S mice ($n = 4$). **D**: NMNAT enzyme activity in MIN6 cells stably transfected with the indicated plasmids. In this and other panels of this figure, Wld^S-H112A stands for EGFP-Wld^S-H112A. **E**: Wld^S upregulated insulin expression dependent on its enzyme activity. Insulin expression in MIN6 cells stably transfected with the indicated plasmids were stained with anti-insulin antibody. In the right panel anti-Wld^S antibody was added to visualize the Wld^S protein. DAPI was used to stain the nuclei. Scale bar, 5 μm . **F**: Insulin content in MIN6 cells stably transfected with the indicated plasmids. **G**: NMNAT enzyme activity was increased in the pancreas of Wld^S mice (11-week-old male mice, $n = 3$ for each genotype). **H**: Insulin mRNA levels of islets isolated from Wld^S mice increased compared with wild-type as determined by real-time PCR ($n = 3$ for each genotype). **I**: Wld^S heightened insulin mRNA levels dependent on its enzyme activity as determined by real-time PCR with MIN6 cells stably transfected with the indicated plasmids. **J** and **K**: Wld^S enhanced insulin promoter activity in a dose-dependent manner (**J**) and required its enzyme activity (**K**). INS-1 cells transfected with pGL3-Insulin-Promoter, and the indicated plasmids were used for luciferase assay to measure insulin promoter activity. * $P < 0.05$ and ** $P < 0.01$. (A high-quality digital representation of this figure is available in the online issue.)

The effect of Wld^S on the upregulation of insulin content in islets was not significant (Fig. 5C), which might be because of the very high insulin levels in normal islets. Insulin expression was increased in MIN6 cells stably expressing EGFP-fused Wld^S or Wld^S with Myc-tag, whereas the increase was attenuated in cells stably expressing Wld^S-H112A or Wld^S-F116S, in which the NAD biosynthesis activity of Wld^S was abolished (Fig. 5D-F). The protein levels of Wld^S and Wld^S/NMNAT1 protein ratio in the cell lines were even higher than those in the islets of

Wld^S mice (Supplementary Fig. 5). Moreover, increased NAD biosynthesis activity was observed in the pancreas of Wld^S mice (Fig. 5G). In addition, Wld^S dramatically upregulated insulin mRNA levels, which also depended on its enzyme activity (Fig. 5H and I). Further studies showed Wld^S activated insulin promoter in a dose-dependent manner, which also required its enzyme activity (Fig. 5J and K). NMNAT1, the COOH-terminal of Wld^S protein, also activated insulin promoter as Wld^S, whereas its enzyme-dead mutant NMNAT1-F28S could not (Fig. 5K). These data suggest that the

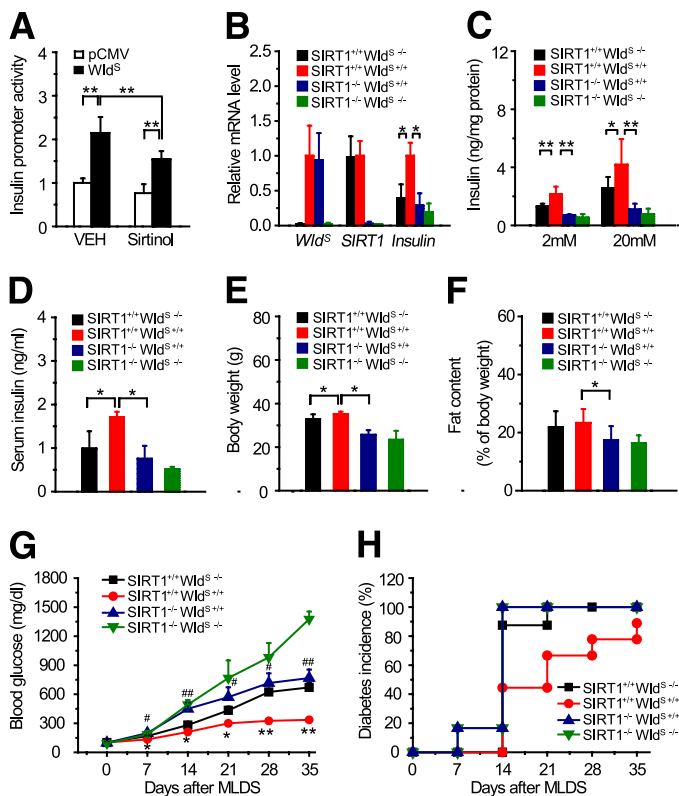


FIG. 6. SIRT1 is required for the enhancement of insulin transcription, secretion, and the resistance to STZ-induced hyperglycemia caused by Wld^S. **A:** Sirtinol attenuated the activation of insulin promoter induced by Wld^S. INS-1 cells were transfected with pGL3-Insulin-Promoter and the indicated plasmids and treated with or without 60 μ M Sirtinol for 24 h for luciferase assay. **B and C:** Upregulation of insulin transcription and insulin secretion by Wld^S required SIRT1. Islets with the indicated genotypes were used for determination of insulin mRNA levels by real-time PCR (**B**) and measurement of insulin secretion at the indicated concentration of glucose (**C**; $n = 4-8$ for each genotype). **D:** Serum insulin levels were significantly attenuated in 15-week-old SIRT1^{-/-} Wld^{S/+} mice compared with SIRT1^{+/+} Wld^{S/+} mice ($n = 5-9$ for each genotype). **E and F:** Body weight and fat content of 10-week-old SIRT1^{-/-} Wld^{S/+} mice were decreased compared with SIRT1^{+/+} Wld^{S/+} mice ($n = 6-11$ for each genotype). **G and H:** Blood glucose (**G**) and diabetes incidence (**H**) of mice with the indicated genotypes after MLDS treatment at the indicated times ($n = 6-9$ for each genotype). Error bars indicate SEM. * $P < 0.05$, ** $P < 0.01$ vs. SIRT1^{+/+} Wld^{S/-}; # $P < 0.05$, ## $P < 0.01$ vs. SIRT1^{+/+} Wld^{S/+}. For diabetes incidence, SIRT1^{+/+} Wld^{S/+} vs. SIRT1^{-/-} Wld^{S/-}, $P < 0.05$; SIRT1^{+/+} Wld^{S/+} vs. SIRT1^{-/-} Wld^{S/+}, $P < 0.05$ by Log-rank test. (A high-quality color representation of this figure is available in the online issue.)

upregulated NMNAT enzyme activity contributes to the enhanced insulin transcription and secretion induced by Wld^S.

SIRT1 is required for the enhanced transcription, secretion of insulin, and the resistance to STZ-induced hyperglycemia caused by Wld^S. We next investigated whether the effect of Wld^S on insulin production and glucose homeostasis depended on SIRT1. Sirtinol, an inhibitor of SIRT1, attenuated Wld^S-induced activation of insulin promoter (Fig. 6A). Insulin transcription and secretion in islets and serum insulin levels of SIRT1^{-/-} Wld^{S/+} mice were significantly decreased compared with SIRT1^{+/+} Wld^{S/+} mice (Fig. 6B-D). The blood glucose levels of SIRT1^{-/-} Wld^{S/+} mice were similar with SIRT1^{+/+} Wld^{S/+} mice no matter whether mice were fed, fasted, or challenged with glucose (Supplementary Fig. 6A-C), which might be as a result of the enhanced insulin sensitivity of SIRT1 null mice (10). The body weight and fat content of SIRT1^{-/-} Wld^{S/+}

mice were decreased compared with SIRT1^{+/+} Wld^{S/+} mice (Fig. 6E and F), probably resulting from their increased energy expenditure (Supplementary Fig. 6D-H). After MLDS treatment, the blood glucose levels of SIRT1^{-/-} Wld^{S/+} and SIRT1^{+/+} Wld^{S/-} mice increased much faster than those of SIRT1^{+/+} Wld^{S/+} mice (Fig. 6G). And the diabetes incidence of SIRT1^{-/-} Wld^{S/+} mice was much higher than that of SIRT1^{+/+} Wld^{S/+} mice (Fig. 6H). Therefore, SIRT1 is necessary for the enhancement of insulin transcription, secretion, and the resistance to STZ-induced hyperglycemia caused by Wld^S.

Wld^S downregulates UCP2 expression and upregulates ATP levels through SIRT1. Next, we explored how Wld^S exerts its function through SIRT1. NMNAT1 was reported to interact with and regulate the activity of SIRT1 in breast cancer cells (33), suggesting Wld^S containing the full-length NMNAT1 has similar effects. As expected, we found Wld^S colocalized and coimmunoprecipitated with SIRT1 (Fig. 7A-C). Besides that, both NAD and its precursor NMN were upregulated in the pancreas of Wld^S mice (Fig. 7D-F), suggesting the activity of SIRT1 was enhanced. SIRT1 has been reported to enhance GSIS by downregulation of UCP2 and upregulation of ATP (10,11). Similarly, we found Wld^S downregulated UCP2 promoter activity like SIRT1 (Fig. 7G) and repressed UCP2 protein and mRNA levels dependent on its NAD biosynthesis activity (Fig. 7C and H). The effect of Wld^S on UCP2 mRNA and protein levels also depended on SIRT1 (Fig. 7I-K). Furthermore, ATP levels were also significantly increased at both low and high glucose concentrations in islets of Wld^S mice compared with wild-type (Fig. 7L), and this function again depended on SIRT1 (Fig. 7M).

DISCUSSION

Over the past decade, numerous studies have focused on the axon protective function of Wld^S and its potential application in neuronal diseases (16). The effect of Wld^S in nonneuronal cells would also probably shed light on the understanding and treating of other diseases. However, there were few reports concerning this. In this study, we demonstrate that Wld^S enhances insulin transcription and secretion as well as improves glucose homeostasis, and SIRT1 is required in these processes.

It is well established that β -cells show a variety of similarities with neuronal cells (34), which implicates that Wld^S, a protein functional in neuronal cells, may also function in β -cells. As expected, we found that Wld^S was highly expressed in the pancreas including insulin-producing β -cells (Fig. 1A-C) and enhanced insulin transcription and secretion (Fig. 5). In addition, Wld^S mice exhibited increased serum insulin levels (Figs. 2A and 3I), even though their blood glucose levels were normal in the fed state (Fig. 2B). Similarly, SIRT4 knockout mice, for example, also show high insulin and normal fed blood glucose levels (35), which might be as a result of the existence of factors that increase blood glucose levels, including glucagon and gluconeogenesis. These factors acted as a counterbalance to neutralize the glucose-lowering effect of insulin and thus to maintain the blood glucose at a stable level. Wld^S mice showed improved glucose tolerance (Fig. 2E). Similarly, β -cell-specific SIRT1-overexpressing mice also show improved glucose tolerance as a result of enhanced GSIS (11). Compatibly, we found that SIRT1 was required for the function of Wld^S in insulin secretion (Fig. 6C and D). Increased cellular NAD levels have been shown to enhance

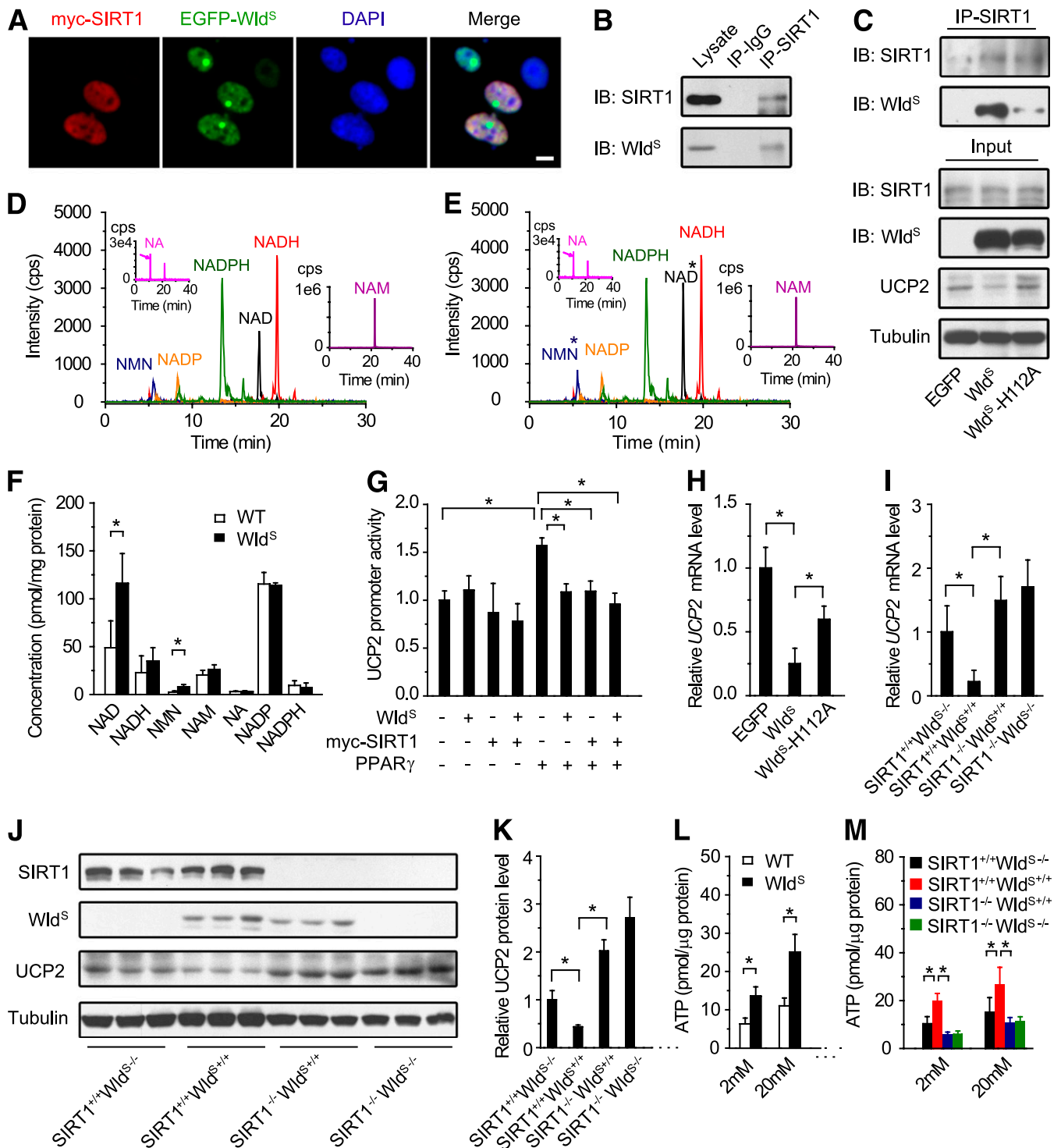


FIG. 7. *Wld^S* downregulates UCP2 expression and upregulates ATP levels through SIRT1. **A:** *Wld^S* colocalized with SIRT1 in MIN6 cells. The stable cell lines expressing EGFP-*Wld^S* were transiently transfected with pCMV-myc-SIRT1 and stained with anti-Myc antibody and DAPI. Scale bar, 5 μ m. **B:** *Wld^S* was coimmunoprecipitated with SIRT1 from the pancreatic lysates of *Wld^S* mice. **C:** *Wld^S* and its enzyme-dead mutant *Wld^S-H112A* coimmunoprecipitated with SIRT1. The MIN6 cells stably expressing EGFP, EGFP-*Wld^S*, or EGFP-*Wld^S-H112A* were used for immunoprecipitation. UCP2 protein levels were also detected by Western blot. **D and E:** Liquid chromatography-tandem mass spectrometry analysis of NMN, NADP, NADPH, NAD, NADH, NA, and NAM extracted from pancreas of 9-week-old wild-type (WT) (**D**) or *Wld^S* mice (**E**). *With significant difference. **F:** Quantification of the small molecules corresponding to **D** and **E** showed that NAD and NMN levels were upregulated in the pancreas of *Wld^S* mice ($n = 4$ for each genotype). **G:** *Wld^S* repressed UCP2 promoter activity like SIRT1. UCP2 promoter activity was measured by luciferase assay in 293T cells transfected with pGL3-UCP2-Promoter and the indicated plasmids. **H:** *Wld^S* downregulated UCP2 mRNA levels dependent on its enzyme activity. UCP2 mRNA level was measured by real-time PCR with MIN6 cell lines stably expressing EGFP, EGFP-*Wld^S*, and EGFP-*Wld^S-H112A*. **I:** *Wld^S* downregulated UCP2 mRNA levels via SIRT1. UCP2 mRNA levels were determined by real-time PCR using islets isolated from mice with the indicated genotype ($n = 4$ for each genotype). **J:** *Wld^S* downregulated UCP2 protein levels via SIRT1. The protein levels in brown fat tissue with the indicated genotype were detected with SIRT1, *Wld^S*, UCP2, and tubulin antibodies ($n = 3$ for each genotype). **K:** Quantification of the UCP2 protein levels corresponding to **J**. **L:** *Wld^S* increased ATP levels in primary cultured islets at the indicated glucose concentration ($n = 3$). **M:** *Wld^S* upregulated ATP level in islets via SIRT1. ATP levels were measured in islets with indicated genotypes at 2 mmol/L or 20 mmol/L glucose ($n = 3$). * $P < 0.05$ and ** $P < 0.01$. (A high-quality digital representation of this figure is available in the online issue.)

SIRT1 activity (6). Consistently, we found NAD and its precursor NMN were upregulated in the pancreas of Wld^S mice (Fig. 7D–F), and Wld^S enhanced insulin transcription dependent on its NAD biosynthesis activity (Fig. 5). These data suggest that NAD plays a key role in SIRT1-mediated enhancement of GSIS induced by Wld^S. It is noteworthy that NMNAT2, an enzyme catalyzing NAD biosynthesis, is highly expressed in the islets of Langerhans (36), which also suggests the importance of NAD biosynthesis in insulin secretion. It has been reported that UCP2 knockout mice show improved GSIS (37), and β -cell-specific SIRT1-overexpressing mice show improved GSIS by decreasing UCP2 expression and elevating ATP levels (11). Analogously, we found Wld^S downregulated UCP2 expression and upregulated ATP levels via SIRT1 (Fig. 7), which further confirmed that Wld^S regulates insulin secretion through a SIRT1-dependent pathway.

Usually, β -cells will secrete more insulin to overcome the reduced insulin sensitivity, which is often related with obesity (38). When their compensate mechanisms are impaired, type 2 diabetes occurs (1). Wld^S mice show increased serum insulin levels no matter whether mice were fed chow or HF diet without altering insulin sensitivity (Fig. 3I–K), which indicates enhanced β -cell function in Wld^S. Furthermore, when fed HF diet, the glucose tolerance of Wld^S mice was strikingly improved (Fig. 3L and M). Similarly, ghrelin knockout mice or GPR40 β -cell-specific transgenic mice also show increased insulin secretory capacity without altering insulin sensitivity and improved glucose tolerance when fed HF diet (39,40). In addition, Wld^S promoted insulin secretion and downregulated UCP2 via SIRT1 (Figs. 6C and 7I–K), which consisted with the studies that both β -cell-specific SIRT1-overexpressing mice and UCP2 knockout mice showed enhanced insulin secretion and resistance to HF diet-induced glucose intolerance (18,41). Taken together, our findings suggest that enhanced insulin secretory capacity by upregulating NAD biosynthesis activity in β -cells would be beneficial to overcome reduced insulin sensitivity induced by HF diet.

Type 1 diabetes is a chronic autoimmune disease, during which β -cells are selectively destroyed (2). MLDS has been extensively used to generate β -cell destruction to mimic type 1 diabetes (25). In this study, we found that MLDS-induced hyperglycemia was alleviated in Wld^S mice, which also demonstrated increased serum insulin levels (Fig. 4). It is noteworthy that UCP2 knockout mice, which showed enhanced insulin secretory capacity, had accelerated hyperglycemia after MLDS treatment as a result of stronger inflammation (24). In this scenario, Wld^S mice were superior to UCP2 knockout mice, probably resulting from some different underlying mechanisms. It has been reported that Wld^S shows protective effects in some neurodegenerative disease models (12,16). It is likely that amelioration of MLDS-induced hyperglycemia and attenuation of neurodegenerative diseases by Wld^S could share some common underlying mechanisms. Additionally, the resistance to MLDS-induced hyperglycemia was abolished in Wld^S mice with SIRT1 deficiency (Fig. 6G and H), which is consistent with the report that intra-arterial targeted islet-specific expression of SIRT1 protects β -cells from STZ-induced apoptosis in mice (42). Thereby, the SIRT1-dependent Wld^S pathway is a potential target not only to enhance insulin secretory capacity, but also to protect against β -cell failure.

In this study, our results demonstrate that Wld^S combines an insulinotropic effect with protection against β -cell

failure and suggest that upregulation of the NAD biosynthesis to increase SIRT1 activity in β -cells will be beneficial for diabetes.

ACKNOWLEDGMENTS

This research was supported by grants from the National Natural Science Foundation of China (30825009, 30970619, 31030022, 81021002, and 30900250), the National Basic Research Program of China (973 Program, 2009CB918403 and 2007CB914501), the National Science and Technology Support Program (2009BAI80B04), the Program of Shanghai Subject Chief Scientist (11XD1405800), the Director Foundation of the Institute for Nutritional Sciences (20090101), SA-SIBS Scholarship Program, the China Postdoctoral Science Foundation (20100480641 and 20080440658), the Postdoctoral Research Program of Shanghai Institutes for Biological Sciences, the Chinese Academy of Sciences (2011KIP511), and the Shanghai Postdoctoral Scientific Program (11R21417400).

No potential conflicts of interest relevant to this article were reported.

J.W. designed the research, performed research, analyzed data, and wrote the manuscript. F.Z., M.Y., D.W., Q.Y., Y.Z., and B.Z. performed research. M.W.M. provided the SIRT1^{+/-} mice and revised the manuscript. Q.Z. designed the research, analyzed data, and wrote the manuscript.

The authors thank all members of the laboratory for sharing reagents and advice.

REFERENCES

- Muoio DM, Newgard CB. Mechanisms of disease: molecular and metabolic mechanisms of insulin resistance and beta-cell failure in type 2 diabetes. *Nat Rev Mol Cell Biol* 2008;9:193–205
- Lehuen A, Diana J, Zaccane P, Cooke A. Immune cell crosstalk in type 1 diabetes. *Nat Rev Immunol* 2010;10:501–513
- Kahn SE, Hull RL, Utzschneider KM. Mechanisms linking obesity to insulin resistance and type 2 diabetes. *Nature* 2006;444:840–846
- Blander G, Guarente L. The Sir2 family of protein deacetylases. *Annu Rev Biochem* 2004;73:417–435
- Finkel T, Deng CX, Mostoslavsky R. Recent progress in the biology and physiology of sirtuins. *Nature* 2009;460:587–591
- Haigis MC, Sinclair DA. Mammalian sirtuins: biological insights and disease relevance. *Annu Rev Pathol* 2010;5:253–295
- Rodgers JT, Lerin C, Haas W, Gygi SP, Spiegelman BM, Puigserver P. Nutrient control of glucose homeostasis through a complex of PGC-1 α and SIRT1. *Nature* 2005;434:113–118
- Sun C, Zhang F, Ge X, et al. SIRT1 improves insulin sensitivity under insulin-resistant conditions by repressing PTP1B. *Cell Metab* 2007;6:307–319
- Kitamura YI, Kitamura T, Kruse JP, et al. FoxO1 protects against pancreatic beta cell failure through NeuroD and MafA induction. *Cell Metab* 2005;2:153–163
- Bordone L, Motta MC, Picard F, et al. Sirt1 regulates insulin secretion by repressing UCP2 in pancreatic beta cells. *PLoS Biol* 2006;4:e31
- Moynihhan KA, Grimm AA, Plueger MM, et al. Increased dosage of mammalian Sir2 in pancreatic beta cells enhances glucose-stimulated insulin secretion in mice. *Cell Metab* 2005;2:105–117
- Coleman M. Axon degeneration mechanisms: commonality amid diversity. *Nat Rev Neurosci* 2005;6:889–898
- Coleman MP, Conforti L, Buckmaster EA, et al. An 85-kb tandem triplication in the slow Wallerian degeneration (Wlds) mouse. *Proc Natl Acad Sci USA* 1998;95:9985–9990
- Conforti L, Tarlton A, Mack TG, et al. A Ufd2/D4Cole1e chimeric protein and overexpression of Rbp7 in the slow Wallerian degeneration (WldS) mouse. *Proc Natl Acad Sci USA* 2000;97:11377–11382
- Mack TG, Reiner M, Beirowski B, et al. Wallerian degeneration of injured axons and synapses is delayed by a Ube4b/Nmnat chimeric gene. *Nat Neurosci* 2001;4:1199–1206
- Coleman MP, Freeman MR. Wallerian degeneration, wld(s), and nmnat. *Annu Rev Neurosci* 2010;33:245–267
- Wang J, Zhai Q, Chen Y, et al. A local mechanism mediates NAD-dependent protection of axon degeneration. *J Cell Biol* 2005;170:349–355

18. Ramsey KM, Mills KF, Satoh A, Imai S. Age-associated loss of Sirt1-mediated enhancement of glucose-stimulated insulin secretion in beta cell-specific Sirt1-overexpressing (BESTO) mice. *Aging Cell* 2008;7:78–88
19. Revollo JR, Körner A, Mills KF, et al. Nampt/PBEF/Visfatin regulates insulin secretion in beta cells as a systemic NAD biosynthetic enzyme. *Cell Metab* 2007;6:363–375
20. McBurney MW, Yang X, Jardine K, et al. The mammalian SIR2alpha protein has a role in embryogenesis and gametogenesis. *Mol Cell Biol* 2003;23:38–54
21. Mi W, Conforti L, Coleman MP. Genotyping methods to detect a unique neuroprotective factor (Wld(s)) for axons. *J Neurosci Methods* 2002;113:215–218
22. Zehetner J, Danzer C, Collins S, et al. PVHL is a regulator of glucose metabolism and insulin secretion in pancreatic beta cells. *Genes Dev* 2008;22:3135–3146
23. Levy JC, Matthews DR, Hermans MP. Correct homeostasis model assessment (HOMA) evaluation uses the computer program. *Diabetes Care* 1998;21:2191–2192
24. Emre Y, Hurtaud C, Karaca M, Nubel T, Zavala F, Ricquier D. Role of uncoupling protein UCP2 in cell-mediated immunity: how macrophage-mediated insulinitis is accelerated in a model of autoimmune diabetes. *Proc Natl Acad Sci USA* 2007;104:19085–19090
25. Burkart V, Wang ZQ, Radons J, et al. Mice lacking the poly(ADP-ribose) polymerase gene are resistant to pancreatic beta-cell destruction and diabetes development induced by streptozocin. *Nat Med* 1999;5:314–319
26. Jia H, Yan T, Feng Y, Zeng C, Shi X, Zhai Q. Identification of a critical site in Wld(s): essential for Nmnat enzyme activity and axon-protective function. *Neurosci Lett* 2007;413:46–51
27. Jin Q, Zhang F, Yan T, et al. C/EBPalpha regulates SIRT1 expression during adipogenesis. *Cell Res* 2010;20:470–479
28. Ge X, Jin Q, Zhang F, Yan T, Zhai Q. PCAF acetylates beta-catenin and improves its stability. *Mol Biol Cell* 2009;20:419–427
29. Whelan JA, Russell NB, Whelan MA. A method for the absolute quantification of cDNA using real-time PCR. *J Immunol Methods* 2003;278:261–269
30. Caruso R, Campolo J, Dellanoce C, Mariele R, Parodi O, Accinni R. Critical study of preanalytical and analytical phases of adenine and pyridine nucleotide assay in human whole blood. *Anal Biochem* 2004;330:43–51
31. Klawitter J, Schmitz V, Klawitter J, Leibfritz D, Christians U. Development and validation of an assay for the quantification of 11 nucleotides using LC/LC-electrospray ionization-MS. *Anal Biochem* 2007;365:230–239
32. Like AA, Rossini AA. Streptozotocin-induced pancreatic insulinitis: new model of diabetes mellitus. *Science* 1976;193:415–417
33. Zhang T, Berrocal JG, Frizzell KM, et al. Enzymes in the NAD⁺ salvage pathway regulate SIRT1 activity at target gene promoters. *J Biol Chem* 2009;284:20408–20417
34. Corbett J, Serup P, Bonner-Weir S, Nielsen JH. Beta-cell ontogeny: growth and death. *Diabetologia* 1997;40(Suppl. 3):B27–B32
35. Haigis MC, Mostoslavsky R, Haigis KM, et al. SIRT4 inhibits glutamate dehydrogenase and opposes the effects of calorie restriction in pancreatic beta cells. *Cell* 2006;126:941–954
36. Yalowitz JA, Xiao S, Biju MP, et al. Characterization of human brain nicotinamide 5'-mononucleotide adenylyltransferase-2 and expression in human pancreas. *Biochem J* 2004;377:317–326
37. Zhang CY, Baffy G, Perret P, et al. Uncoupling protein-2 negatively regulates insulin secretion and is a major link between obesity, beta cell dysfunction, and type 2 diabetes. *Cell* 2001;105:745–755
38. Biddinger SB, Kahn CR. From mice to men: insights into the insulin resistance syndromes. *Annu Rev Physiol* 2006;68:123–158
39. Dezaki K, Sone H, Koizumi M, et al. Blockade of pancreatic islet-derived ghrelin enhances insulin secretion to prevent high-fat diet-induced glucose intolerance. *Diabetes* 2006;55:3486–3493
40. Nagasumi K, Esaki R, Iwachidow K, et al. Overexpression of GPR40 in pancreatic β -cells augments glucose-stimulated insulin secretion and improves glucose tolerance in normal and diabetic mice. *Diabetes* 2009;58:1067–1076
41. Joseph JW, Koshkin V, Zhang CY, et al. Uncoupling protein 2 knockout mice have enhanced insulin secretory capacity after a high-fat diet. *Diabetes* 2002;51:3211–3219
42. Tang MM, Zhu QE, Fan WZ, et al. Intra-arterial targeted islet-specific expression of Sirt1 protects β cells from streptozotocin-induced apoptosis in mice. *Mol Ther* 2011;19:60–66